Electronic Supplementary Material (ESI) for Dalton Transactions.

Mechanistic insights on the non-innocent role of the electron donor: reversible photocapture of CO_2 by Ru^{II}-polypyridyl complexes

Supplementary Information

N. Queyriaux,* W. B. Swords, H. Agarwala, B. A. Johnson, S. Ott, and L. Hammarström

All reagents were purchased from Sigma-Aldrich or TCI Europe and used as obtained unless otherwise stated. Reagent-grade solvents were used without further purification.

[Ru(^{t}Butpy)(dmbpy)Cl](PF_6) (1-Cl). Ru(^{t}Bu$_3$-tpy)Cl$_3$ (100 mg, 0.164 mmol), 4,4′-dimethyl-2,2'-bipyridine (30 mg, 0.164 mmol), LiCl (35 mg, 0.820 mmol) and triethylamine (37 µL) were refluxed overnight in degassed EtOH/H_2O mixture (20 mL, 3:1), under argon. Solvents were evaporated under reduced pressure and the residue was suspended in 20 mL of water. After addition of 2 mL of a saturated aqueous solution of NH_4PF_6, the suspension was stirred for 30 min. The resulting precipitate was collected, thoroughly washed with H_2O and dried under vacuum overnight. The crude product was then subjected to a two-step purification procedure. Firstly, purified by chromatography on alumina (toluene / acetonitrile, 50:50), the desired compound was then eluted from a second chromatography on silica (acetone / 10 % saturated NH_4PF_6 solution, 98:2). The major purple band was collected and concentrated under reduced pressure precipitating out the desired product, which was collected, washed with H_2O, and dried under vacuum overnight (107 mg, ρ = 75%).
^{1}H NMR (400 MHz, acetone-*d6*): δ 10.11 (d, *J* = 5.7 Hz, 1H), 8.79 (s, 2H), 8,69 (s, 1H), 8.67 (d, *J* = 2.0 Hz, 2H), 8.42 (s, 1H), 7.85 (d, *J* = 5.8 Hz, 1H), 7.64 (d, *J* = 5.9 Hz, 2H), 7.35 (dd, *J* = 5.9, 2.0 Hz, 2H), 7.29 (d, *J* = 5.9 Hz, 1H), 6.88 (d, *J* = 6.0 Hz, 1H), 2.34 (s, 3H), 2.06 (s, 3H), 1.59 (s, 9H), 1.33 (s, 18H).

[Ru(tpy)(bpy)(MeCN)](PF_6) (1-MeCN). 1-Cl (85 mg, 0.098 mmol) was dissolved in degassed MeCN/H_2O mixture (2:1, 60 mL) and refluxed under argon overnight. Acetonitrile was evaporated under reduced pressure and a few drops of a saturated aqueous solution of NH_4PF_6 was added to the solution. The resulting suspension was stirred for 30 min. The bright orange precipitate was collected, thoroughly washed with H_2O and dried under vacuum overnight (74 mg, ρ = 74%).
^{1}H NMR (400 MHz, acetone-*d6*): δ 9.70 (d, *J* = 5.7 Hz, 1H), 8.97 (s, 2H), 8.84 (d, *J* = 1.8 Hz, 2H), 8.80 (s, 1H), 8.54 (s, 1H), 7.93 (d, *J* = 4.9 Hz, 1H), 7.84 (d, *J* = 5.9 Hz, 2H), 7.51 (dd, *J* = 5.9, 2.1 Hz, 2H), 7.35 (d, *J* = 5.9 Hz, 1H), 7.03 (d, *J* = 4.9 Hz, 1H), 2.40 (s, 3H), 2.32 (s, 3H), 1.62 (s, 9H), 1.37 (s, 18H).

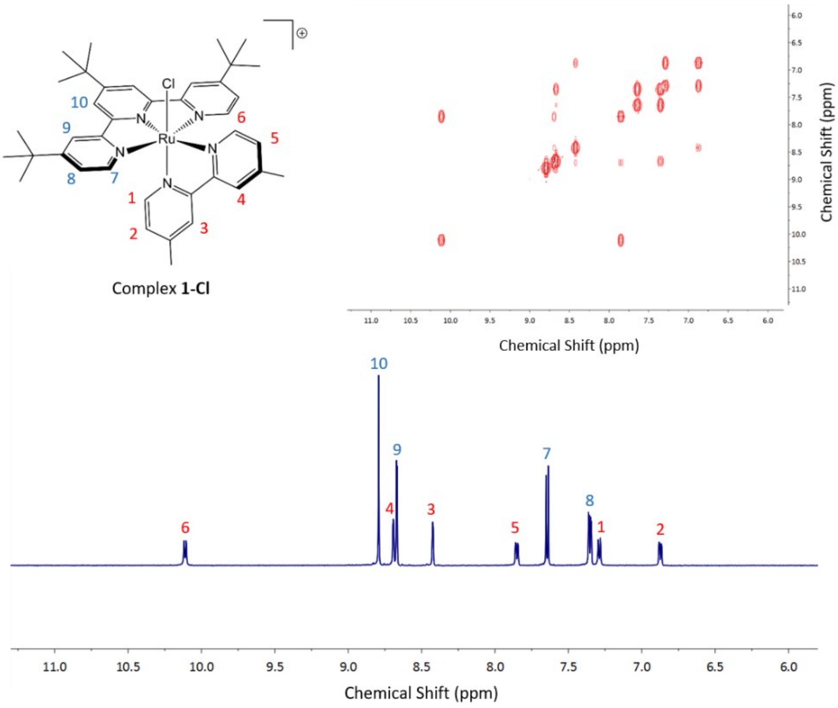

Figure S1. Aromatic region (11.3 – 5.8 ppm) of the ^{1}H-NMR and COSY spectra of **1-Cl** in acetone-*d6*.

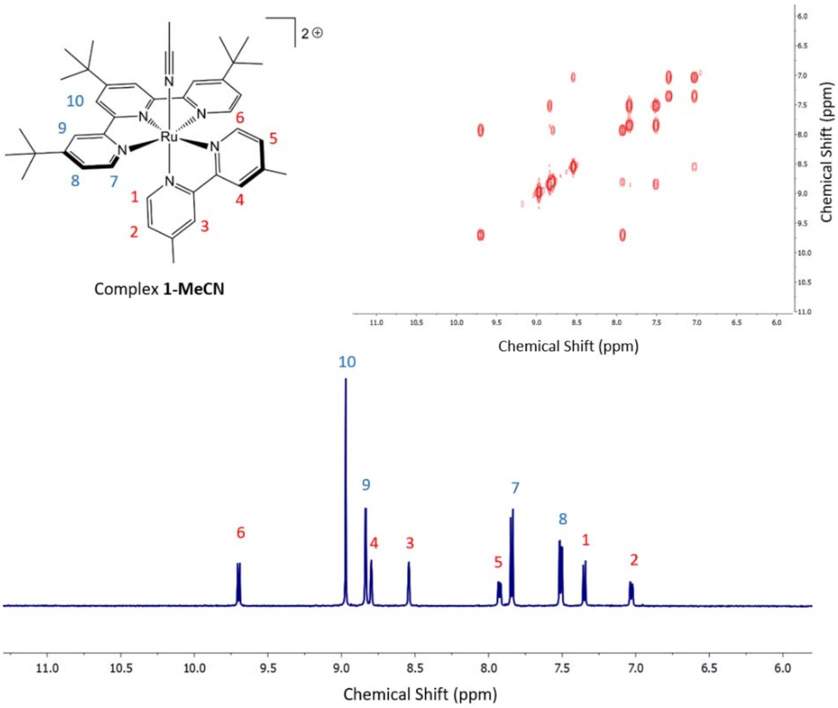

Figure S2. Aromatic region (11.3 – 5.8 ppm) of the ^{1}H-NMR and COSY spectra of **1-MeCN** in acetone-*d6*.

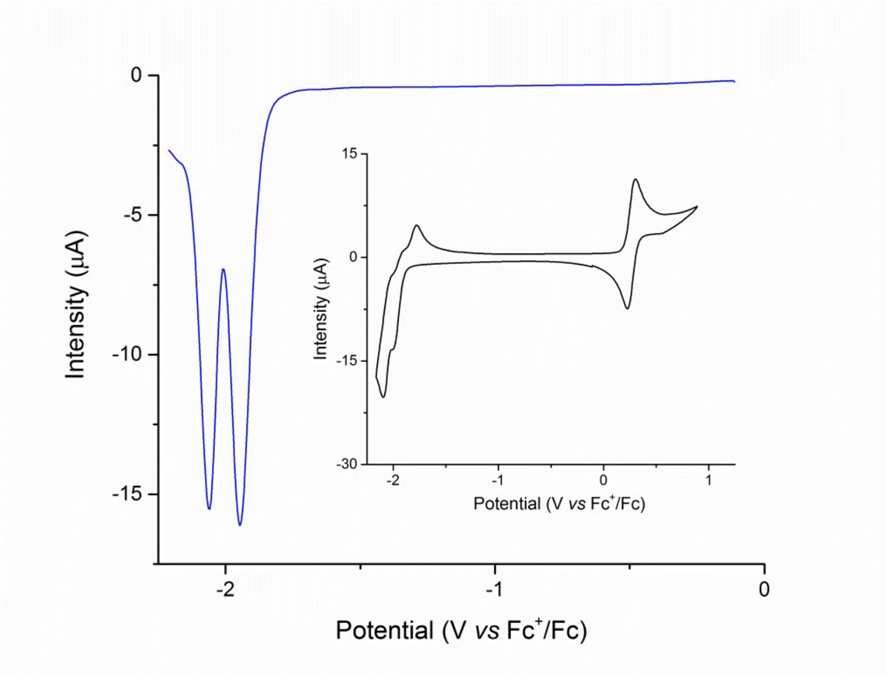

Figure S3. Differential pulse voltammogram (blue trace) and cyclic voltammogram at 50 mV.s^{-1} (black trace, insert) of 0.75 mM solution of **1-Cl**, recorded in MeCN (containing 0.1 M n-Bu$_4$NPF$_6$ as supporting electrolyte) under Ar atmosphere. Setup: glassy carbon working electrode, Pt counter-electrode and Ag/AgNO$_3$ reference electrode. DPV parameters: Step Potential 5 mV, Pulse Amplitude 25 mV, Pulse Periode 0.1s and Pulse Width 0.05s.

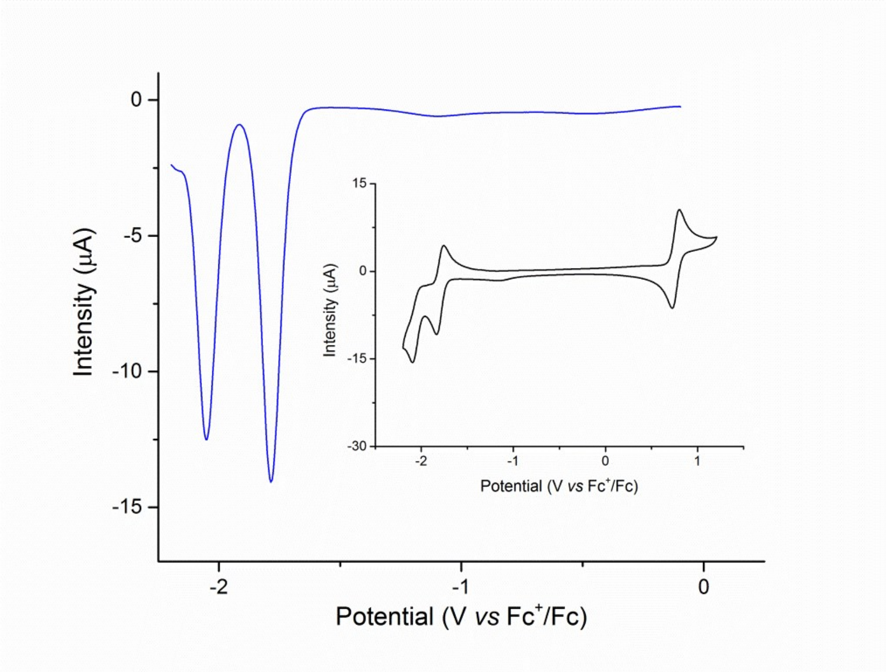

Figure S4. Differential pulse voltammogram (blue trace) and cyclic voltammogram at 50 mV.s^{-1} (black trace, insert) of 0.75 mM solution of **1-MeCN**, recorded in MeCN (containing 0.1 M n-Bu$_4$NPF$_6$ as supporting electrolyte) under Ar atmosphere. Setup: glassy carbon working electrode, Pt counter-electrode and Ag/AgNO$_3$ reference electrode. DPV parameters: Step Potential 5 mV, Pulse Amplitude 25 mV, Pulse Periode 0.1s and Pulse Width 0.05s.

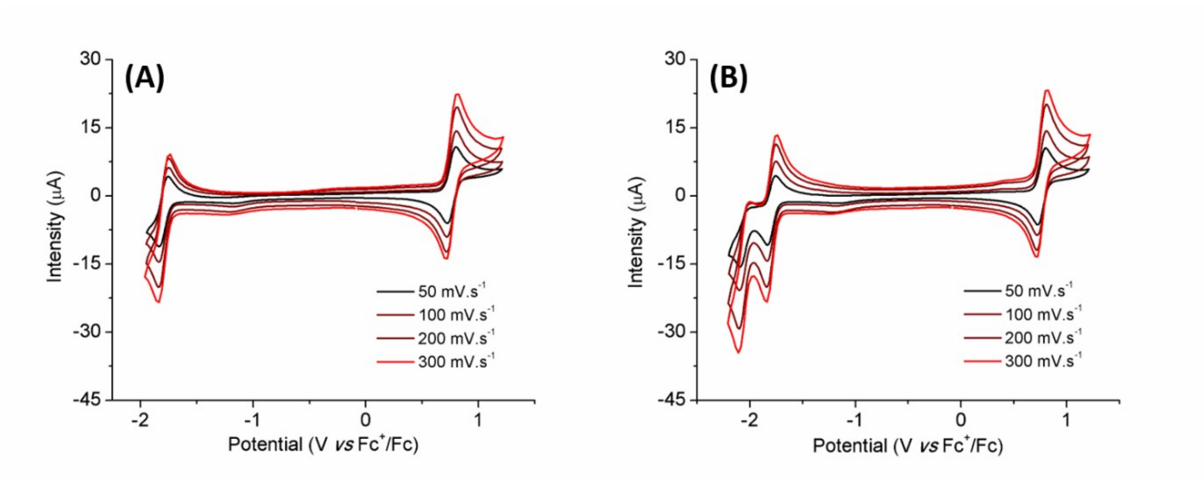

Figure S5. Cyclic voltammograms of 0.75 mM solution of **1-MeCN**, recorded at increasing scan rate (from 50 mV.s^{-1} to 300 mV.s^{-1}) in MeCN (containing 0.1 M n-Bu$_4$NPF$_6$ as supporting electrolyte) under Ar atmosphere: (A) between 1.2 V and -1.95V *vs* Fc$^+$/Fc and (B) between 1.2 V and -2.2 V *vs* Fc$^+$/Fc . Setup: glassy carbon working electrode, Pt counter-electrode and Ag/AgNO$_3$ reference electrode.

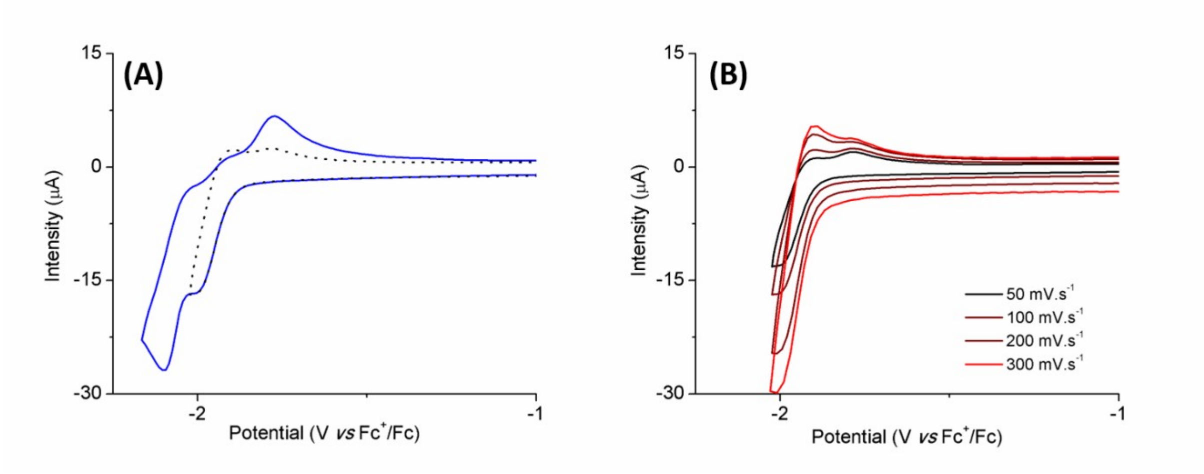

Figure S6. (A) Comparison of the cathodic part of the cyclic voltammograms of 0.75 mM solution of **1-Cl** when potential is switched back after the second reduction process (plain blue trace) or the first reduction process (dashed black trace) and **(B)** Scan rate dependence of the reoxidation processes when potential is switched back after the first reduction (from 50 mV.s-1 to 300 mV.s-1). Voltammograms were recorded in MeCN (containing 0.1 M n-Bu$_4$NPF$_6$ as supporting electrolyte) under Ar atmosphere. Setup: glassy carbon working electrode, Pt counter-electrode and Ag/AgNO$_3$ reference electrode.

Ligand photosubstitution quantum yield determination

A 20 µM solution of **1-MeCN** in Ar-deaerated DMF (3mL in 10x10 mm quartz cuvette, exposed surface of 3 cm²) was irradiated using 466 nm LED light; the power was determined to be 3.14 J.s^{-1}.cm^{-2} by using a powermeter (LM-2-VIS, Coherent). Spectral changes of the solution over the course of irradiation, recorded at intervals of 30 s, are reported in Figure S7. Interestingly, the spectrum recorded at 600 s aligns with the spectrum of the **1-DMF** complex[1]. Clean isosbestic points were observed at 470 nm and 392 nm.

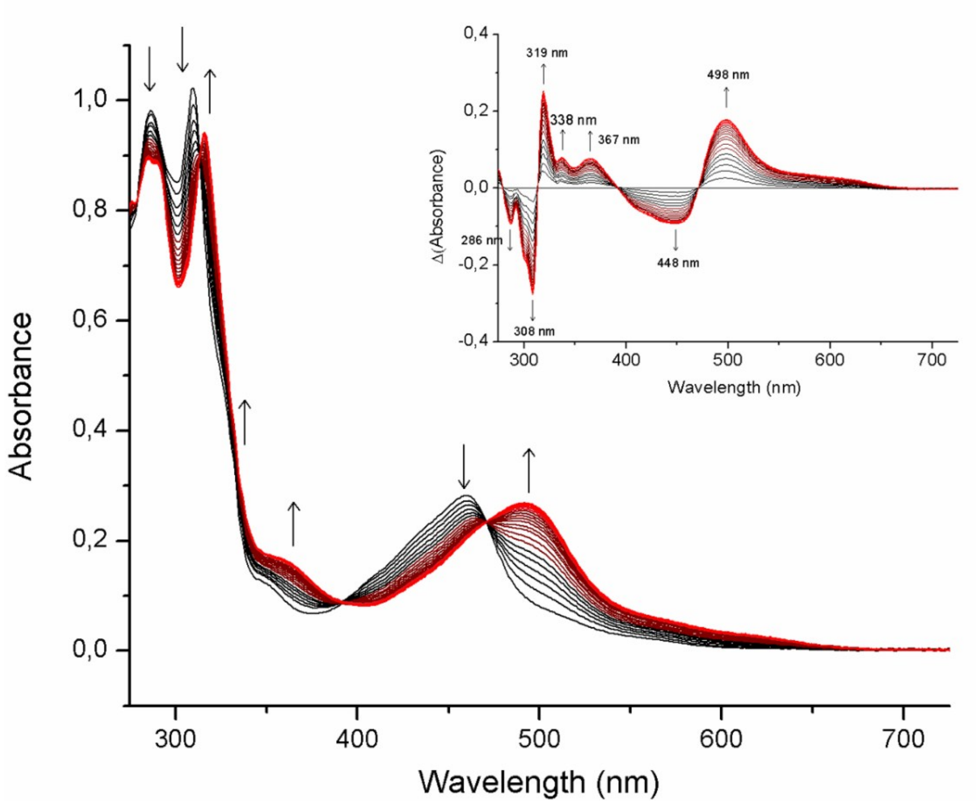

Figure S7. UV-Vis absorption spectra of a 20 µM solution of **1-MeCN** in Ar-deaerated DMF over the course of irradiation at 466 nm (light power, 3.14 J.s^{-1}.cm^{-2}). Spectra were recorded at intervals of 30 seconds over 600 s (from black trace to red trace).

Due to the presence of isosbestic points and to a complete photosubstitution of MeCN ligand within the time range, **1-MeCN** and **1-DMF** concentrations could be monitored over the course of the photolysis experiment using the following equations (eq. S1-S2).

$$[1-MeCN]_t = [1-MeCN]_0 \times \frac{A^{459\,nm}_{f} - A^{459\,nm}_{t}}{A^{459\,nm}_{f} - A^{459\,nm}_{0}} \qquad \text{(eq. S1)}$$

$$[1-DMF]_t = [1-MeCN]_0 \times \frac{A^{494\,nm}_{0} - A^{494\,nm}_{t}}{A^{494\,nm}_{0} - A^{494\,nm}_{f}} \qquad \text{(eq. S2)}$$

where A_t, A_0 and A_f are the absorbance measured at 459 nm or 494 nm, during the photolysis, before the photolysis and after 600 s of photolysis. Figure S8 displays concentrations evolution of both ruthenium complexes during the ligand photosubstitution process. Monoexponential fitting of **1-MeCN** concentration decay and **1-DMF** concentration growth allowed the determination of a reaction observed half-time $t_{1/2} = 161\ s$ for the ligand photosubstitution reaction.

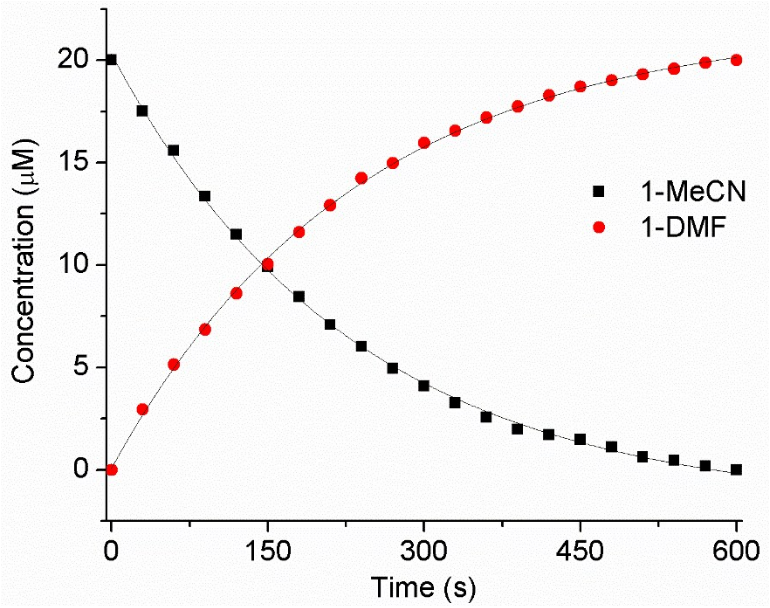

Figure S8. Evolution of **1-MeCN** and **1-DMF** concentrations over the course of a photolysis experiment.

Quantum yield of the overall photosubstitution process was then estimated using the following equation (eq. S3) and initial ($t = 0$) parameters.

$$\Phi = \frac{number\ of\ 1 - DMF\ molecules\ generated\ per\ seconds}{number\ of\ photons\ absorbed\ per\ seconds}$$

$$\Phi = \frac{[1 - MeCN]_0.V.k_{obs}}{I_0\left(1 - 10^{-A_0^{459nm}}\right).S_{irr}} \qquad \text{(eq. S3)}$$

where Φ, $[1 - MeCN]_0$, V, k_{obs}, I_0, A_0^{459nm} and S_{irr} are the quantum yield, the initial concentration of **1-MeCN** (in mol.L^{-1}), the volume of the irradiated solution (in L), the pseudo-first order rate constant (in s^{-1}), the electron flux (in mol. s^{-1}.cm^{-2}), the absorbance at 459 nm before the photolysis started and the surface of irradiation (in cm^{-2}). A quantum yield of 0.011 was finally calculated for the ligand photosubstitution process.

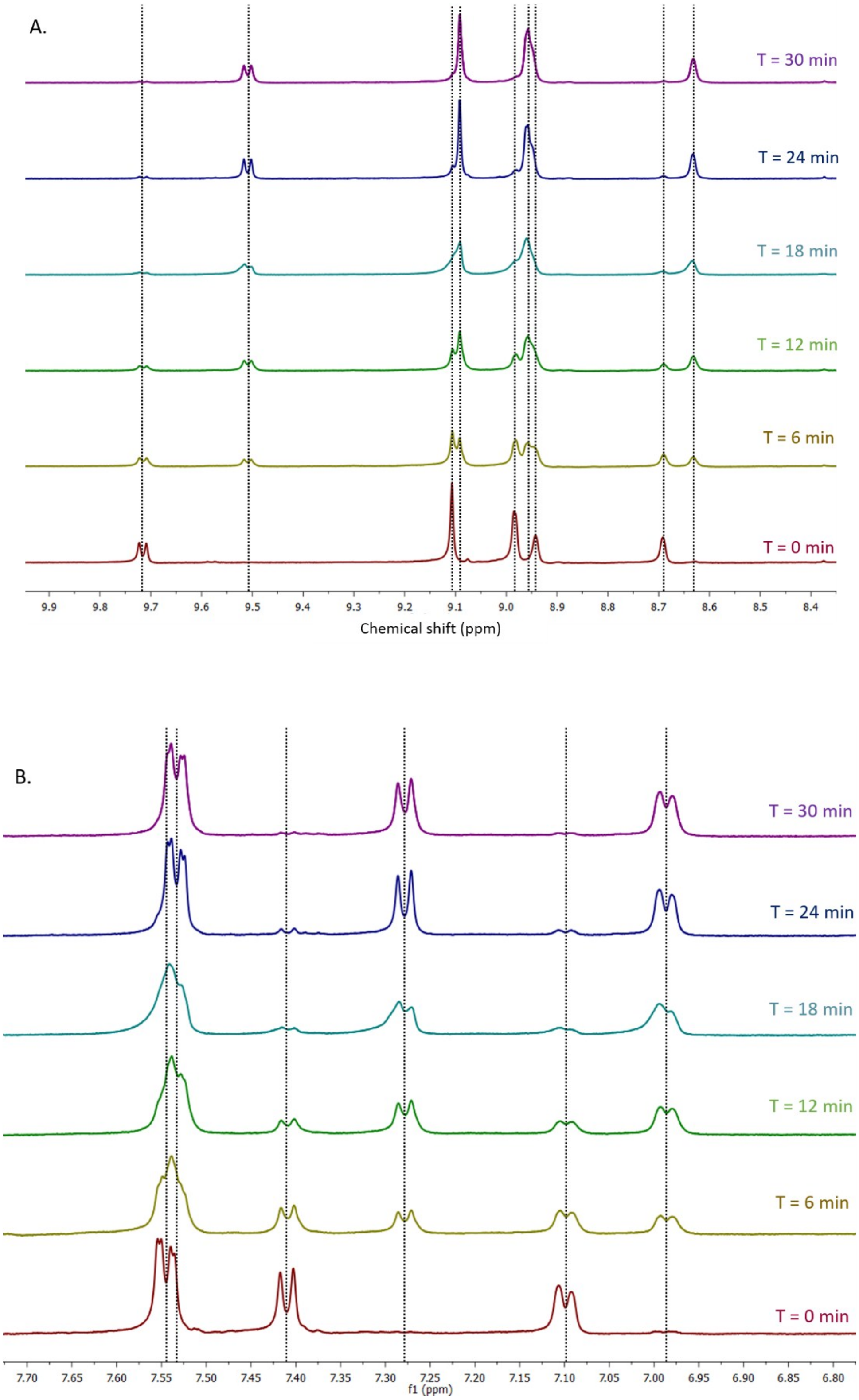

Figure S9. Selected regions of the ^{1}H-NMR spectrum of a 4 mM solution of **1-MeCN** in deuterated DMF over the course of irradiation at 466 nm. (A) From 10 to 8.3 ppm and (B) from 7.75 to 6.75 ppm.

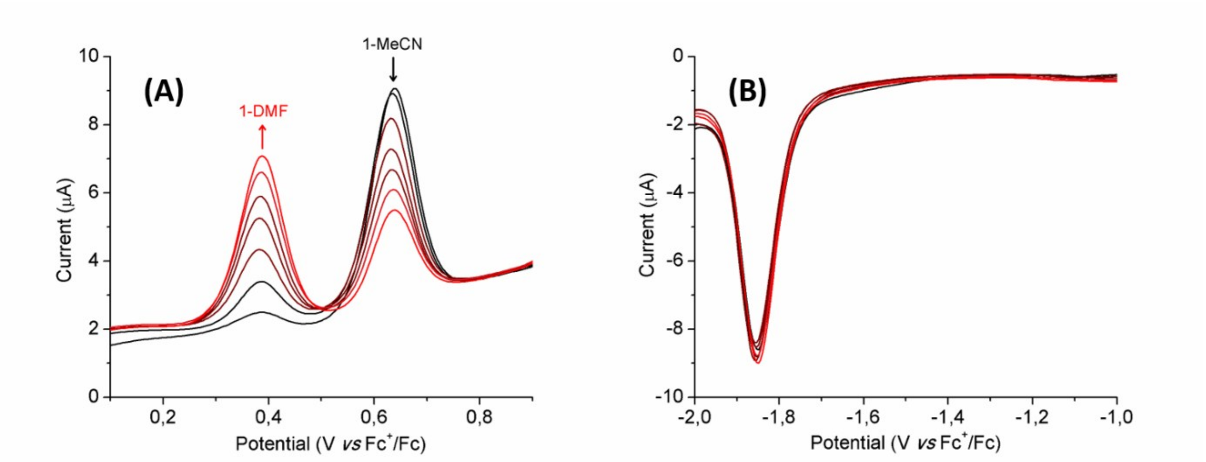

Figure S10. Differential pulse voltammograms of 0.50 mM solution of **1-MeCN**, recorded over the course of irradiation at 466 nm in DMF (containing 0.1 M n-Bu_4NPF_6 as supporting electrolyte) under Ar atmosphere. Voltammograms were recorded at intervals of 10 minutes during 60 min (from black trace to red trace). Setup: glassy carbon working electrode, Pt counter-electrode and Ag/$AgNO_3$ reference electrode. DPV parameters: Step Potential 5 mV, Pulse Amplitude 25 mV, Pulse Periode 0.1s and Pulse Width 0.05s.

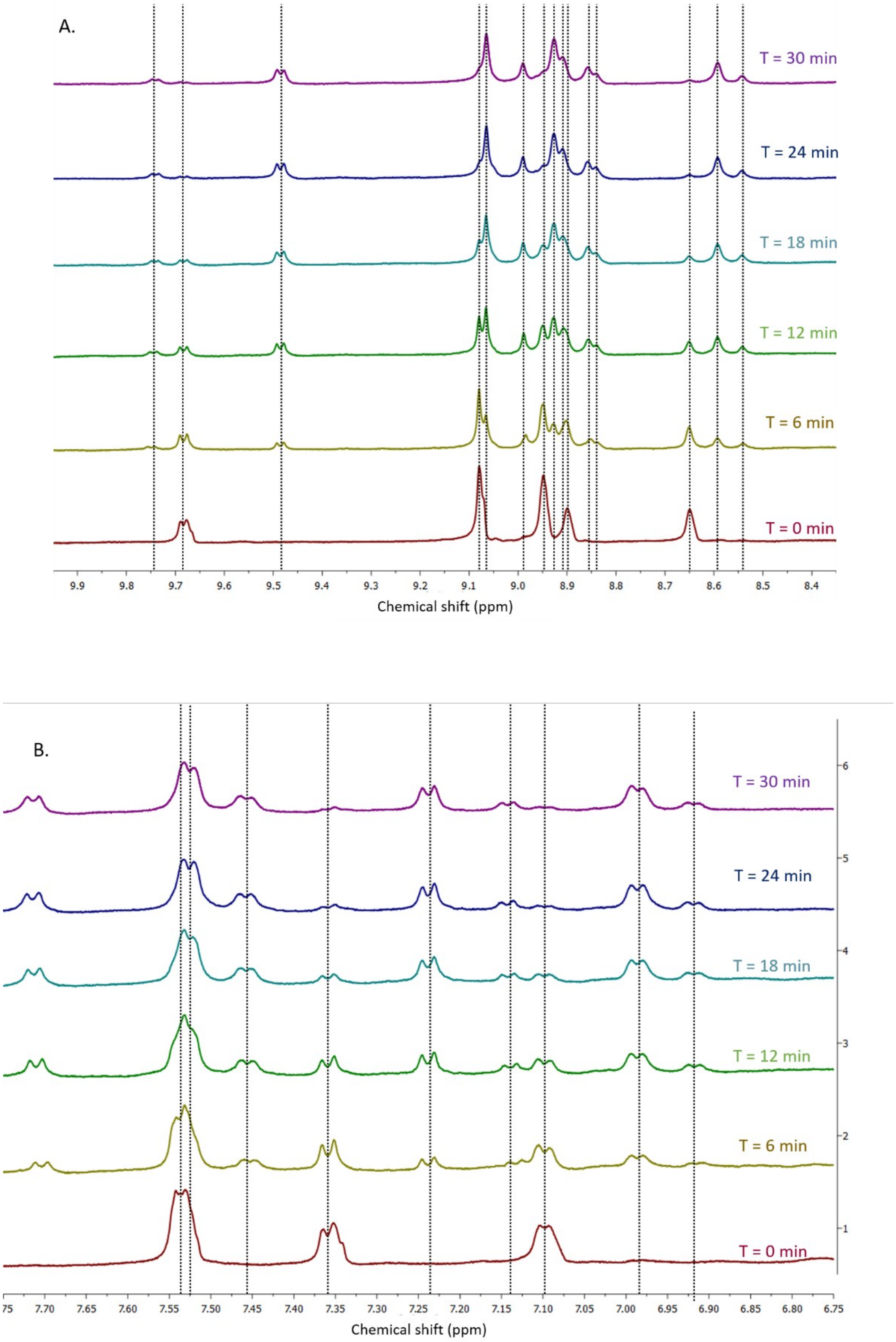

Figure S11. Selected regions of the ^{1}H-NMR spectrum of a 4 mM solution of **1-MeCN** in d*7*-DMF/TEOA (5:1) over the course of irradiation at 466 nm. (A) From 10 to 8.3 ppm and (B) from 7.75 to 6.75 ppm.

Dark equilibrium constant determination

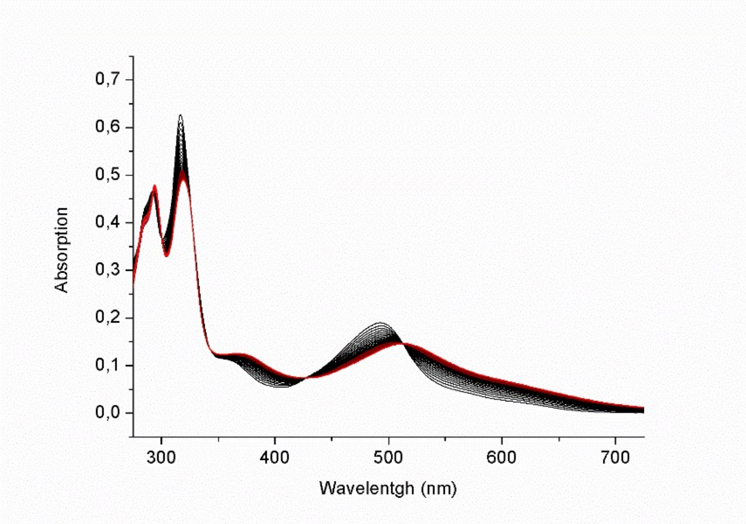

Figure S12. UV-Vis spectral changes of an Ar-saturated DMF solution of freshly photogenerated **1-DMF** (20 µM) when kept in the dark in the presence of TEOA. Spectra were recorded at intervals of 10 minutes over a period of 10h (from black trace to red trace).

NMR tubes containing a 4 mM solution of **1-MeCN** in Ar-deaerated deuterated DMF (400 µL) were irradiated for 1h using 466 nm LED light. The quantitative conversion of **1-MeCN** in **1-DMF** was confirmed by ^{1}H-NMR and no further photodegradation was identified. Increasing amounts of TEOA were then added and the mixture was let in the dark for 24h. Using the peak areas of the signals associated with the two considered species (**1-DMF** and **1-TEOA**), the composition ratio was determined for a series of solvent mixture. Equilibrium constant K_{eq} was then calculated using the slope of Figure S13 and the following equation (eq. S4).

$$K_{eq} = \frac{[1-TEOA].[DMF]}{[1-DMF].[TEOA]} \qquad \text{(eq. S4)}$$

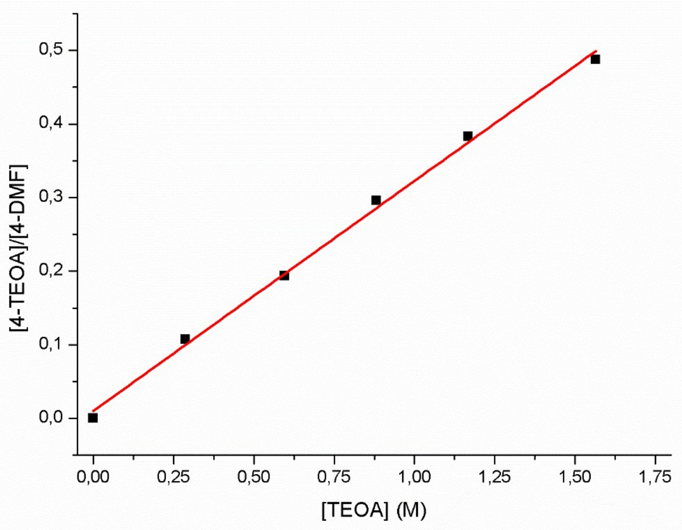

Figure S13. Plot of the evolution of the ratio between the peak areas associated with **1-DMF** and **1-TEOA** as a function of the amount of TEOA in the medium.

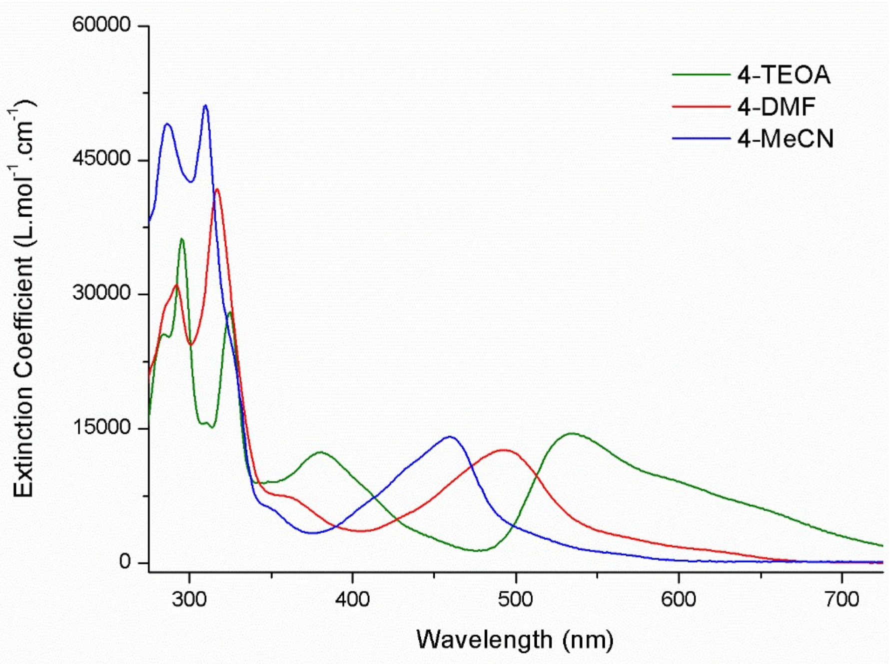

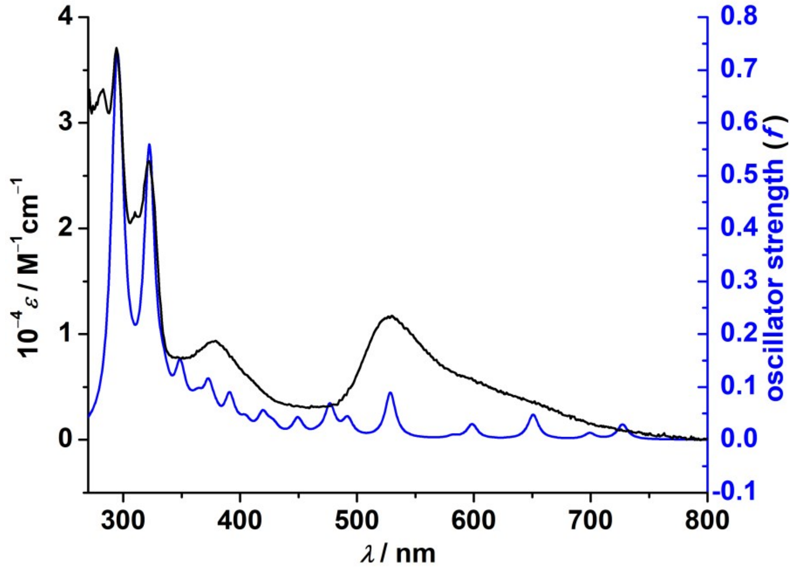

Figure S14. (*Up*) Extinction coefficient spectra of **1-MeCN** (blue trace) and **1-DMF** (red trace), associated with the subtraction-obtained spectrum of **1-TEOA** (green trace). (*Down*) Experimental (black) and TD-DFT calculated (blue) UV-vis spectra of **1-TEOA**.

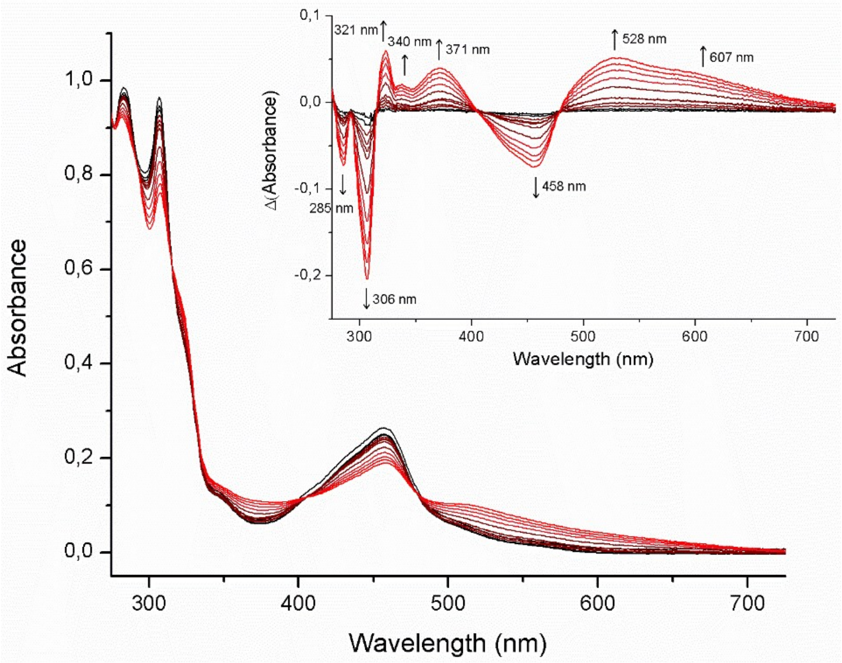

Figure S15. UV-Vis spectral changes under 466 nm LED irradiation of an Ar-deaerated MeCN/TEOA (5:1) solution of **1-MeCN** (20 μM). Spectra were recorded at intervals of 30 seconds (from black trace to red trace).

Speciation of 1-MeCN over the course of a photolysis experiment in DMF/TEOA

The UV-Vis spectra collected during the photolysis of **1-MeCN** in deaerated DMF/TEOA solution were modeled through a linear combination of three components: **1-MeCN**, **1-DMF** and **1-TEOA**, eq S5 and S6. The extinction coefficient of **1-TEOA** was calculated from the ratio of **1-MeCN** to **1-TEOA** determined by NMR analysis. The UV-Vis spectra were modeled over the wavelength range of 320–800 nm with a 1 nm resolution. Higher energy wavelengths (< 320 nm) were not used due to absorption outside the linear range of the spectrometer. With the known extinction coefficient spectra, the coefficients of each species were determined through a least-squares regression performed in Mathematica. As the extinction coefficients ($\varepsilon_{1\text{-}x}$) were utilized to model the data, the coefficients returned corresponded to the concentration of the specific species at the given time point ($c_{1\text{-}x}$). Thus allowing the concentration of the individual species to be quantified during photolysis.

$$A_{Tot} = A_{1-MeCN} + A_{1-DMF} + A_{1-TEOA} \qquad \text{eq S5}$$

$$A_{Tot} = c_{1-MeCN}\varepsilon_{1-MeCN} + c_{1-DMF}\varepsilon_{1-DMF} + c_{1-TEOA}\varepsilon_{1-TEOA} \qquad \text{eq S6}$$

To check the accuracy of these coefficients ($c_{1\text{-}x}$), they along with the extinction coefficient spectra were utilized to simulate the UV-Vis spectra at different time points. These simulations aligned well with the experimental data (Figure S16). As a second check, the low energy region 675 – 800 nm was modeled. Across these wavelengths, only **1-TEOA** absorbs to an appreciable extent. When only the extinction coefficient for **1-TEOA** was utilized to model this wavelength range, the concentration profile was almost identical to that when the full wavelength range was modeled (Figure S17). A third check of this regression analysis was performed through the modeling of a smaller section of the data (400–700 nm). In this region, all three species absorbance overlap appreciably, and the low noise region between 700–800 nm is avoided. The same least-squares regression was utilized to model this region, and both the spectral simulation and concentration profiles aligned with the analysis performed over the entire wavelength range. Finally, attempts to model the spectral changes with just two of the species (**1-MeCN** + **1-DMF**, **1-MeCN** + **1-TEOA**, or **1-DMF** + **1-TEOA**) did not yield accurate results due to large errors in the spectral simulations at nearly all time points (Figure S18).

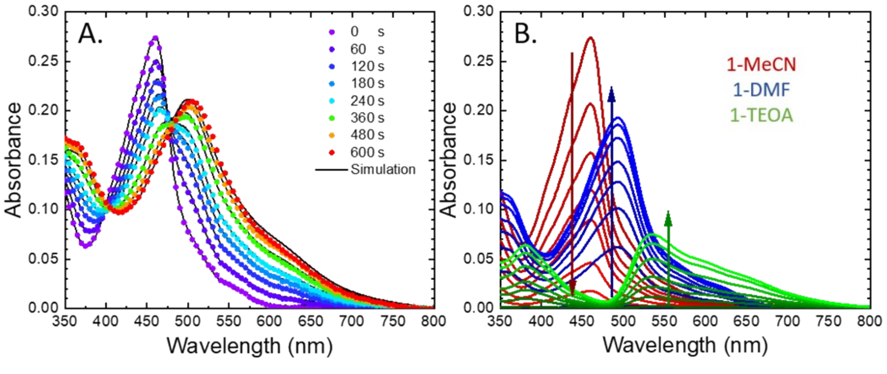

Figure S16. (A) UV-Vis absorption spectra taken at the indicated time delays during the course of the photolysis, circles. The black lines are simulated spectra from a linear combination of the extinction coefficient spectra of the three individual species. (B) The changes in the UV-Vis spectra deconstructed into the absorbance spectra of the three species at the same time delays shown in A. The spectra of **1-MeCN** decays away as **1-DMF** and **1-TEOA** form.

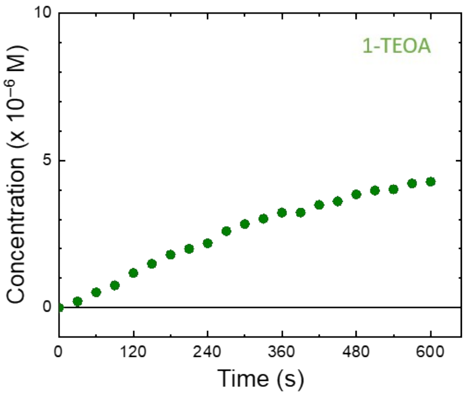

Figure S17. Control simulation concentration profile in which the low energy region (675–800 nm) of the photolysis experiment was modeled with **1-TEOA** only. The concentration profile aligns well with the three component model used to simulate the full wavelength range.

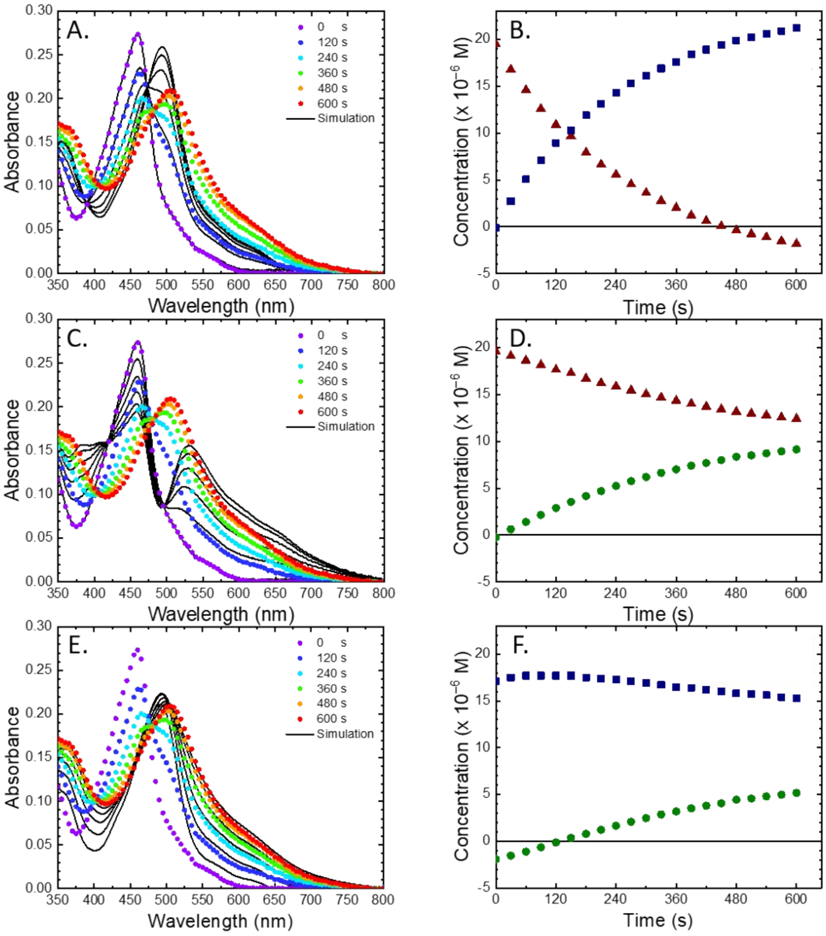

Figure S18. Control simulations (A, C, E) with respective concentration profiles (B, D, F) in which one of the three key spectra have been removed: (A, B) **1-TEOA** removed, (C, D) **1-DMF** removed and (E, F) **1-MeCN** removed. All three spectra are required to adequately model the data throughout the entire course of the photolysis experiment.

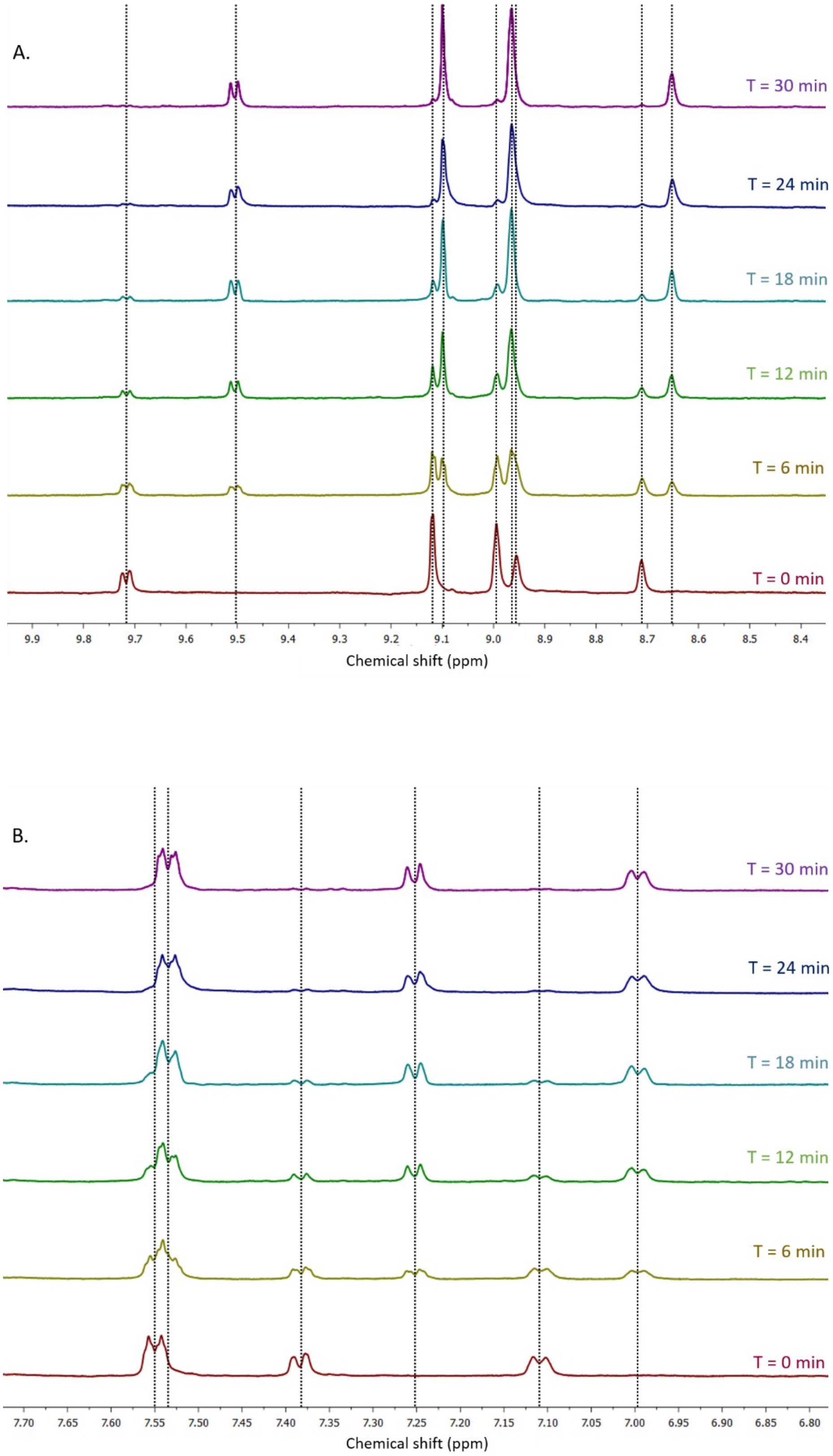

Figure S 19. Selected regions of the ^{1}H-NMR spectrum of a 4 mM solution of **1-MeCN** in d7-DMF/TEA (5:1) over the course of irradiation at 466 nm. (A) From 10 to 8.3 ppm and (B) from 7.75 to 6.75 ppm.

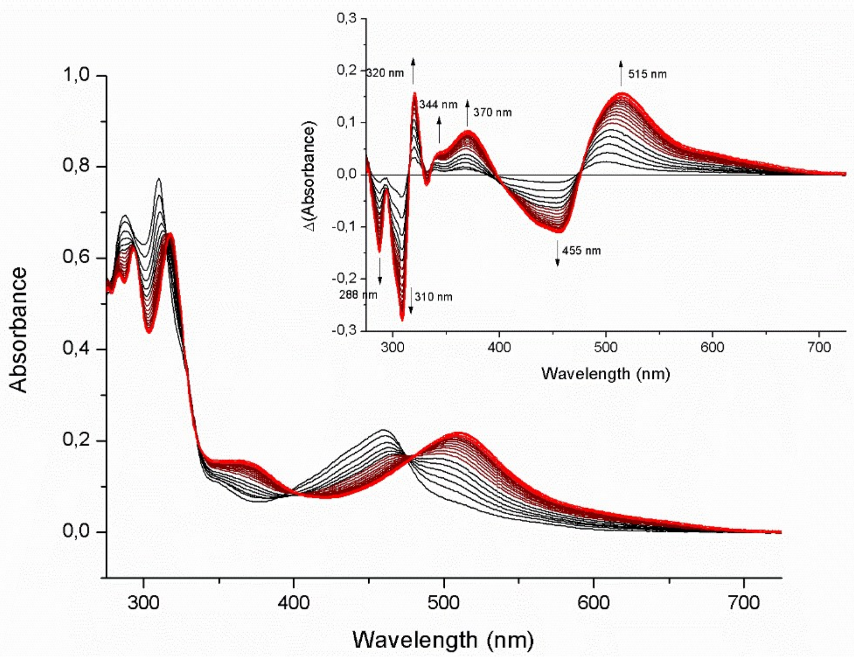

Figure S20. UV-Vis spectral changes under 466 nm LED irradiation of a CO_2-saturated DMF/TEOA (5:1) solution of **1-MeCN** (20 μM). Spectra were recorded at intervals of 30 seconds (from black trace to red trace).

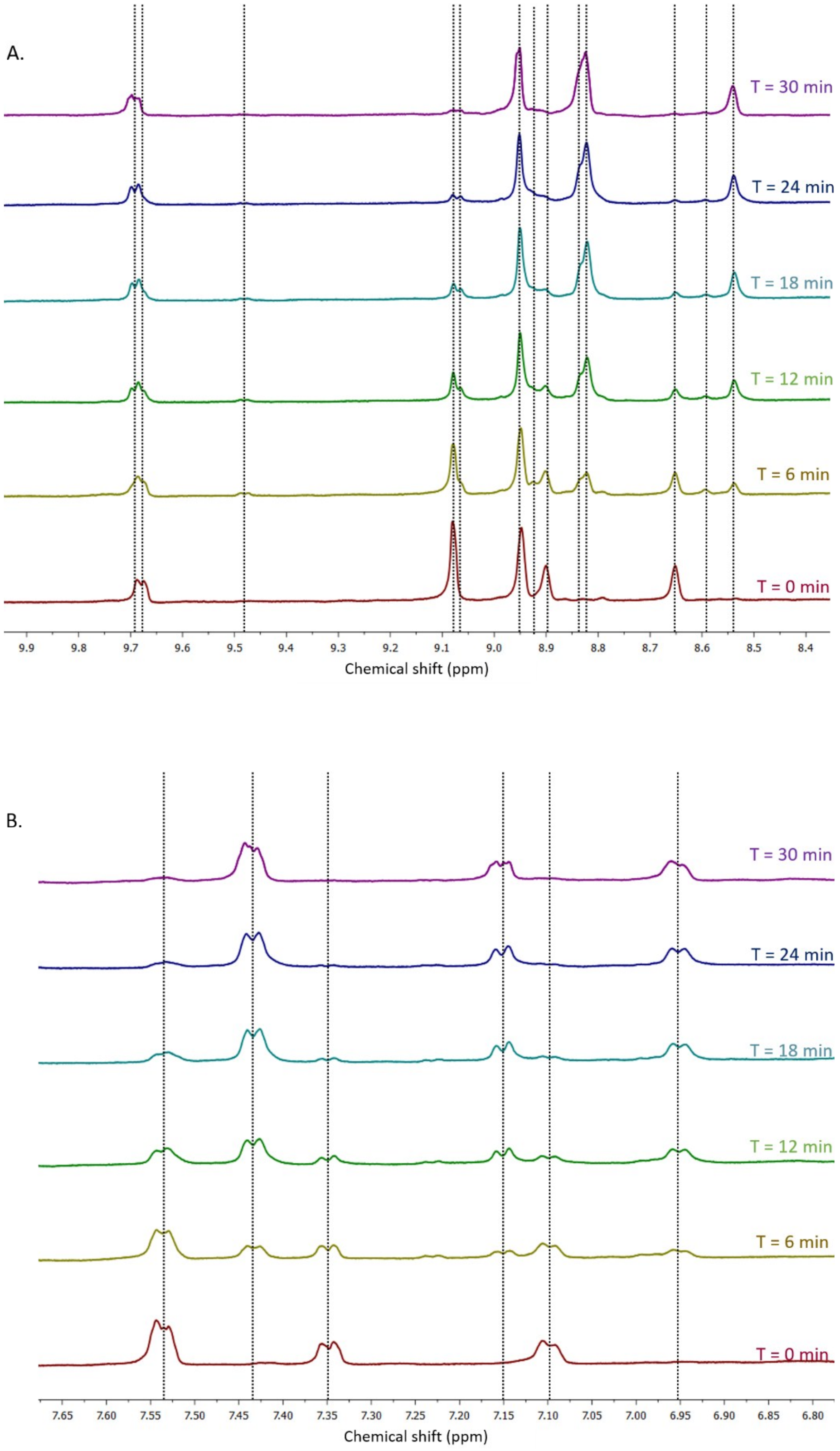

Figure S21. Selected regions of the ^{1}H-NMR spectrum of a 4 mM solution of **1-MeCN** in CO_2-saturated d7-DMF/TEOA (5:1) over the course of irradiation at 466 nm. (A) From 10 to 8.3 ppm and (B) from 7.75 to 6.75 ppm.

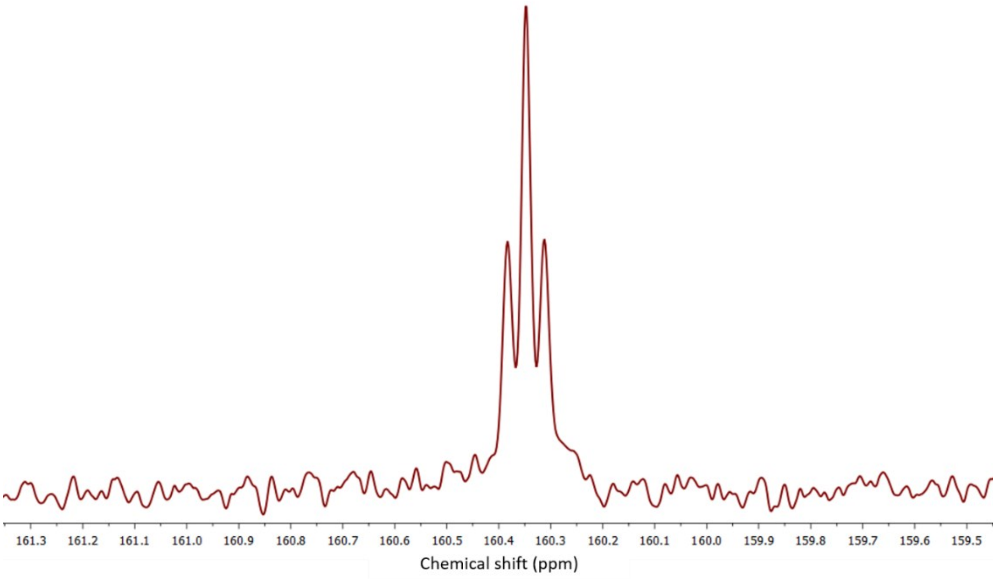

Figure S22. Selected region of the ^{13}C NMR spectrum (without ^{1}H decoupling) of a reactive mixture made of **1-MeCN** in $^{13}CO_2$-saturated d*7*-DMF/TEOA (5:1) after 2h of irradiation at 466 nm.

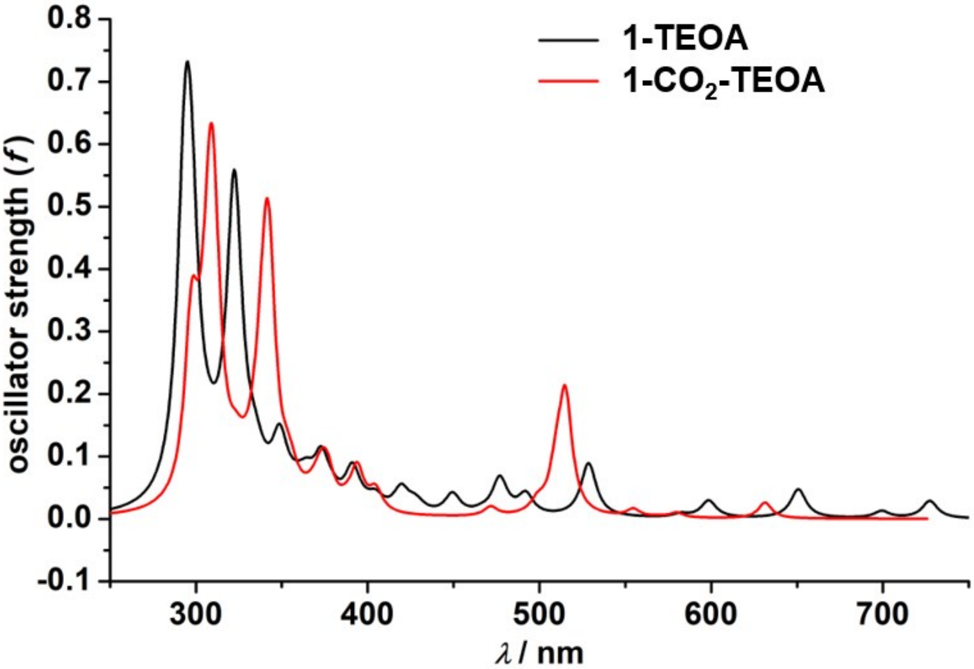

Figure S23. TD-DFT calculated spectra of **1-TEOA** (black trace) and **$1-CO_2-TEOA$** (red trace).

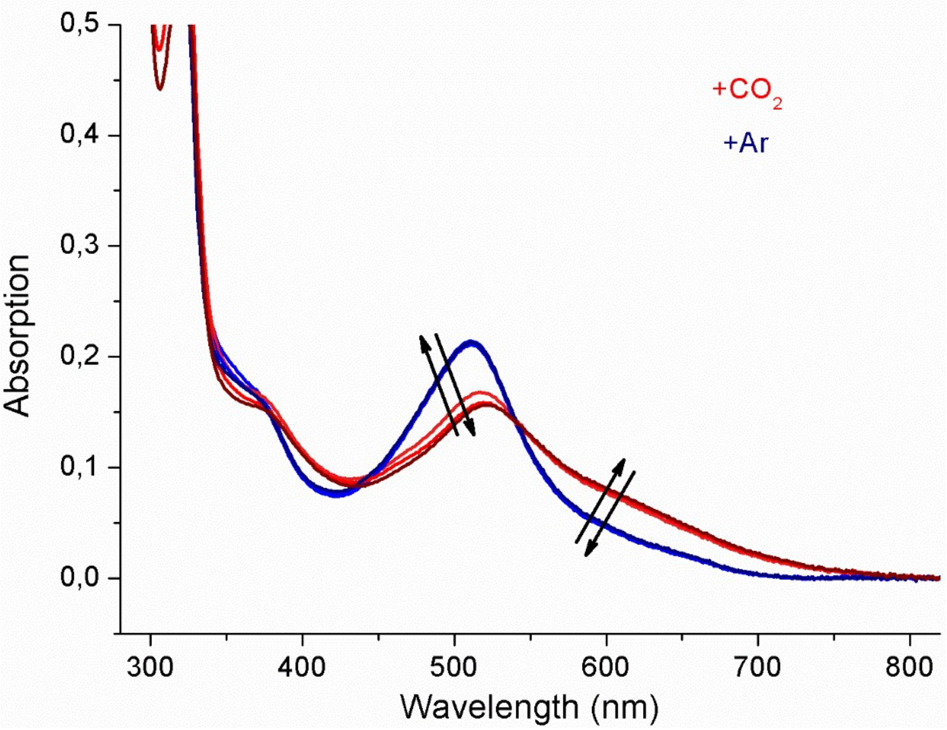

Figure S24. UV-vis spectral changes of a DMF/TEOA (5:1) solution of **4-1MF** (20 µM) upon successive Ar (blue traces) or CO_2 (red traces) 5 min bubbling.

Computational details

Full geometry optimizations were carried out using the density functional theory (DFT) method at the B3LYP level for **4**-X (X = TEOA, CO_2-TEOA).[2] All elements except ruthenium were assigned the 6-31G* basis set. The SDD basis set with effective core potential was employed for the ruthenium atom.[3] Vibrational frequency calculations were performed to ensure that the optimized geometries represent the local minima and there are only positive eigenvalues. All calculations were performed with the Gaussian09 program package.[4] Vertical electronic excitations based on B3LYP optimized geometries were computed for **4**-X (X = TEOA, CO_2-TEOA) using the time-dependent density functional theory (TD-DFT) formalism[5] in N,N-dimethylformamide (DMF) as the solvent, using the conductor-like polarizable continuum model (CPCM).[6] All the calculated structures were visualized with ChemCraft.[7]

References:

1. Matsubara, Y.; Konno, H.; Kobayashi, A.; Ishitani, O., Quantitative Photochemical Formation of [Ru(Tpy)(Bpy)H]+. *Inorganic Chemistry* **2009**, *48*, 10138-10145.
2. C. Lee, W. Yang and R. G. Parr, *Phys. Rev. B.*, 1988, **37**, 785-789.
3. (*a*) D. Andrae, U. Haeussermann, M. Dolg, H. Stoll and H. Preuss, *Theor. Chim. Acta*, 1990, **77**, 123-141; (*b*) P. Fuentealba, H. Preuss, H. Stoll and L.V. Szentpaly, *Chem. Phys. Lett.*, 1989, **89**, 418-422.
4. M. J. Frisch, G. W. Trucks, H. B. Schlegel, G. E. Scuseria, M. A. Robb, J. R. Cheeseman, G. Scalmani, V. Barone, B. Mennucci, G. A. Petersson, H. Nakatsuji, M. Caricato, X. Li, H. P. Hratchian, A. F. Izmaylov, J. Bloino, G. Zheng, J. L. Sonnenberg, M. Hada, M. Ehara, K. Toyota, R. Fukuda, J. Hasegawa, M. Ishida, T. Nakajima, Y. Honda, O. Kitao, H. Nakai, T. Vreven, J. A. Montgomery, J. E. Peralta Jr., F. Ogliaro, M. Bearpark, J. J. Heyd, E. Brothers, K. N. Kudin, V. N. Staroverov, R. Kobayashi, J. Normand, K. Raghavachari, A. Rendell, J. C. Burant, S. S. Iyengar, J. Tomasi, M. Cossi, N. Rega, J. M. Millam, M. Klene, J. E. Knox, J. B. Cross, V. Bakken, C. Adamo, J. Jaramillo, R. Gomperts, R. E. Stratmann, O. Yazyev, A. J. Austin, R. Cammi, C. Pomelli, J. W. Ochterski, R. L. Martin, K. Morokuma, V. G. Zakrzewski, G. A. Voth, P. Salvador, J. J. Dannenberg, S. Dapprich, A. D. Daniels, O. Farkas, J. B. Foresman, J. V. Ortiz, J. Cioslowski and D. J. Fox, Gaussian 09 (Revision A.02): Gaussian, Inc.: Wallingford CT 2009.
5. (*a*) R. Bauernschmitt and R. Ahlrichs, *Chem. Phys. Lett.*, 1996, **256**, 454-464; (*b*) R. E. Stratmann, G. E. Scuseria and M. J. Frisch, *J. Chem. Phys.*, 1998, **109**, 8218-8224; (*c*) M. E. Casida, C. Jamorski, K. C. Casida and D. R. Salahub, *J. Chem. Phys.*, 1998, **108**, 4439-4449.
6. (*a*) V. Barone and M. Cossi, *J. Phys. Chem. A*, 1998, **102**, 1995-2001; (*b*) M. Cossi and V. Barone, *J. Chem. Phys.*, 2001, **115**, 4708-4717; (*c*) M. Cossi, N. Rega, G. Scalmani and V. Barone, *J. Comput. Chem.*, 2003, **24**, 669-681.
7. D. A. Zhurko and G. A. Zhurko, ChemCraft 1.5, Plimus, San Diego, CA. Available at http://www.chemcraftprog.com.